Journal of Materials Chemistry A

Accepted Manuscript

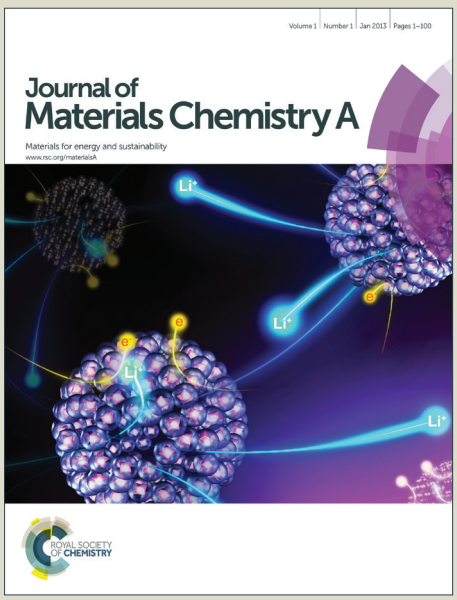

ROYAL SOCIETY OF CHEMISTRY

www.rsc.org/materialsA

Journal of Materials Chemistry A

Cite this: DOI: 10.1039/coxx00000x

www.rsc.org/xxxxxx

Communication

From a polyoxotitanium cage to TiO_2/C composites, a novel strategy to nanoporous materials

Junlei Liu,[a] Zhiwei Cai,[a] Yaokang Lv,[a,b]* Yujian Zhang,[a,c] Chang Su,[a] Mi Ouyang,[a] Cheng Zhang[a,*] and Dominic S. Wright[b,*]

Received (in XXX, XXX) Xth XXXXXXXXX 20XX, Accepted Xth XXXXXXXXX 20XX
DOI: 10.1039/b000000x

A novel strategy to obtain nanoporous titania materials through polyoxotitanium (POT) cages has been developed. Mesoporous and hierarchical nanoporous TiO_2/carbon composites have been fabricated from a new POT cage precursor $[Ti_2O(OAc)_2(HOAc)_2Cl_4]$ and the electrochemical behaviors of these composites were studied.

TiO_2 (titania, titanium dioxide) is an abundant, technologically-important and environmentally-benign semiconductor which has been widely used in photocatalysis, sensors, electrochromic devices and energy storage.[1] Due to theirlong-term chemical and structural stability during reversible Li-intercalation/deintercalation, titania based materials are promising candidates for application in supercapacitors.[2] In order to fabricate novel titania materials, several strategies have been reported, nevertheless there are still great challenges in preparing nanostructured titania with large surface area and controllable pore size.[1a,3] Polyoxotitanium (POT) cages are polynuclear titanium complexes,[4] which not only can be regarded as models for studying bulk titania, but also are useful as organically-soluble single-source precursors for construction of titania materials.[5] We recently reported that sonication and hydrolysis of different POT cages in aqueous ethanol can give titania materials with different properties.[1b] In the current study, a new strategy to obtain nanoporous titania materials through POT is described. Two nanoporous TiO_2/C composites have been obtained *via* calcination of a new POT cage precursor. The electrochemical behaviors of these composites have also been studied.

The liquid phase reaction of $TiCl_4$ with glacial acetic acid in toluene at room temperature yielded large colourless crystals of the new POT cage $[Ti_2O(OAc)_2(HOAc)_2Cl_4]$ (**1**) (ESI). A Single-crystal XRD study revealed that cage **1** has a dinuclear structure in which two Ti centers are associated by two bridging acetate ligands and a μ-O atom. The six-coordinated geometry of each of the symmetry-related Ti centers is completed by two terminal chloride ligands and by bonding to the O-atom of an acetate ligand (Fig. **1**).

Calcination of crystals of cage **1** at 500 °C in air gives an off-white TiO_2/C composite **A**, while calcination of **1** at 500 °C under a purified nitrogen flow gives black TiO_2/C composite **B**. Elemental analysis shows that **A** contains *ca*. 0.16 wt% elemental carbon while **B** contains *ca.* 16.69 wt% carbon (ESI). Powder XRD analysis shows that **A** and **B** are composed of a mixture of amorphous and crystalline material, with the major crystalline phase in both being anatase (ESI).

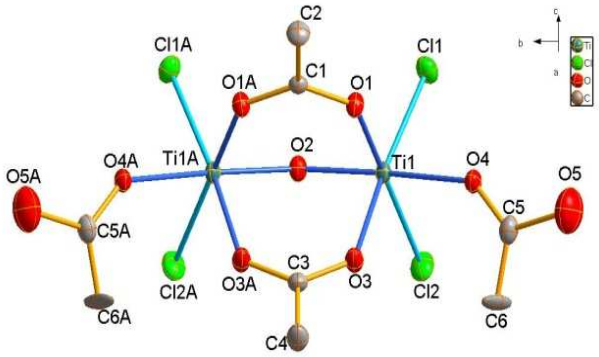

Fig. 1 Solid-state structures of cage **1**. H-atoms (which could not be located from X-ray data) have been omitted for clarity. Selected bond lengths (Å) and angles (°): Ti(1)-O(1) 2.005(2), Ti(1)-O(2) 1.784(1), Ti(1)- O(3) 2.057(3), Ti(1)-O(4) 2.086(2), Ti(1)-Cl(1) 2.243(3), Ti(1)-Cl(2)2.275(4), Cl(1)-Ti(1)-Cl(2) 97.71(5) , Ti(1)-O(2)-Ti (1)137.0(2)

The morphological features of **A** and **B** were characterized by scanning electron microscopy (SEM), transmission electronmicroscopy (TEM), high-resolution TEM (HRTEM) and by their selected area electron diffraction (SAED) patterns. The SEM analysis (Fig. 2) reveals that the average grain size of **B** is significantly smaller than that of **A,** this difference maybe due to the larger amount of carbon in **B** that undermines the accumulation and crystallization of TiO_2 particles. As shown in Fig. 3, the TEM images of **A** and **B** are similar, both samples contain massive disordered nanoscale pores. However, the dark areas in the TEM image of **B** (Fig. 3b) are much more significant than in **A** (Fig. 3a), consistent also with the greater wt% of carbon in **B**. As shown in Fig. 4, the HRTEM image shows that the TiO_2 in both **A** and **B** are crystalline. The lattice fringe spacing was measured to be 0.352 nm, which is consistent with the {101} plane of anatase (JCPDF # 21-1272). The SAED pattern of **A** (Fig. 4a) contains clearly resolved diffraction spots related to anatase and diffraction rings arising from the amorphous component in the sample. The far less well resolved diffraction pattern found for **B** (Fig. 4b) suggests a greater proportion of amorphous components in this sample.

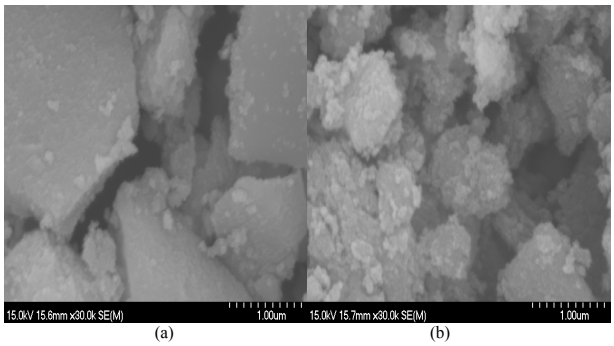

(a) (b)

Fig. 2 SEM images of (a) **A** and (b) **B**.

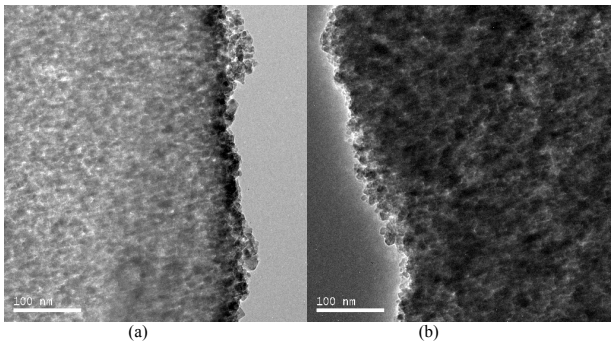

(a) (b)

Fig. 3 TEM images of (a) **A** and (b) **B**.

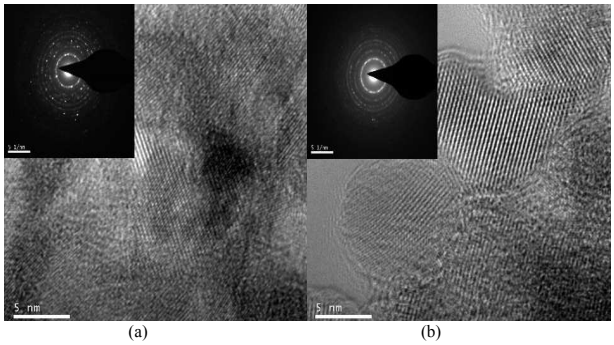

(a) (b)

Fig. 4 HRTEM images of (a) **A** and (b) **B**. The inserts show the SAED patterns.

As shown in the Fig. 5a, The type IV[6] nitrogen sorption isotherms of **A** exhibit a sharp capillary condensation step at relative pressures of 0.4~0.8, corresponding to a narrow pore-size distribution. The Brunauer-Emmett-Teller (BET) surface area of **A** is around 70 m^2g^{-1}, its pore-size distribution, which is calculated from the desorption branch of the isotherm using the Barrett-Joyner-Halenda (BJH) method, exhibits single pores with the most probable pore size of 3.5 nm. In comparison, the isotherms of **B** (Fig. 5b) suggests the existence of hierarchical pore structure with different pore sizes from micro- to mesopores. The BET surface area of **B** is about 110 m^2g^{-1} with the average pore size width of 6.4 nm. The pore sizes found in **B** span the range *ca*. 9.2 to 2.2 nm. The hierarchical structure of **B** is expected to enhance its electrochemical properties as it is desirable for advanced electrode materials for supercapacitors to have a range of pore sizes; mesoporous channels provide low-resistance pathways for ion transport, while micropores strengthen the electric double-layer capacitance.[6b,7]

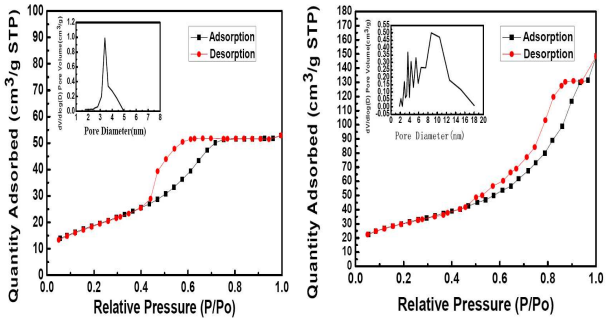

(a) (b)

Fig. 5 Nitrogen adsorption and desorption isotherms and the pore size distributions (insert) of **A** (a) and **B** (b).

The difference in the morphologies of **A** and **B** must result from the calcination processes involved in their formation. As shown in Scheme **1**, calcination in an oxygen-rich environment in the case of **A** results in rapid oxidation of the organic residues present in the precursor **1**, leading to rapid aggregation of the TiO_2 nanoparticles formed and a lower wt% carbon. In the case of **B**, however, the greater carbon content and the more complicated morphology is explained by the slower decomposition of the organic residues in **1** and the agglomeration of carbon regions in the sample. Clearly, the nanostructure and pore size distributions of derived composites are adjustable through alternating the calcination conditions involved.

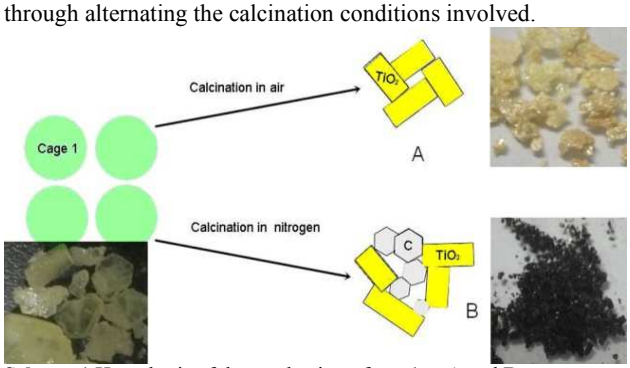

Scheme 1 Hypothesis of the mechanisms from **1** to **A** and **B**.

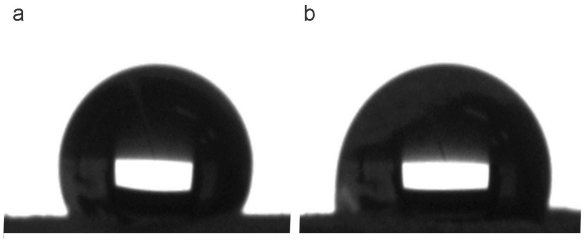

Fig. 6 Photographs of water droplet on the surface of (a) **A** and (b) **B**.

The surface wettability of **A** and **B** have been investigated by measurement of the water contact angles. Fig.**6**. shows the shape of a water droplet on the surface of **A** and **B**. The contact angle of **B** for water is about 115.2°, obviously lower than that of **A** (126.8°), which shows the surface wettability of **B** is better than **A**.

To evaluate the electrochemical properties of **A** and **B**, electrochemical measurements were conducted in a three-electrode electrochemical cell with a platinum counter electrode and an Ag/AgCl reference electrode. Fig. 7 shows the cyclic

voltammogram (CV) curves collected for **A** and **B** electrodes (ESI). As shown in Fig. 7a, a pair of redox peaks attributed to the reversible insertion/removal of Li ions was observed in both curves in propylene carbonate electrolyte. Electrode **A** exhibits cathodic electrochromism[9] (ESI) but the peak cathodic current and peak anodic current of **B** are higher than that of **A**. As shown in Fig. 7b and Fig. 7c, **A** and **B** display different electrochemical behaviors in anaqueous electrolyte. The CV curves of **A** exhibit redox peaks at sweep rates from 10 to 1000 mVs^{-1}; while the CV curves of **B** exhibit a quasi-rectangular shape at sweep rates from 10 to 200 mVs^{-1}, with the absence of any redox peaks, indicating ideal capacitance behavior, but this rectangle behavior changes at sweep rates of 500mVs^{-1} and 1000 mVs^{-1}, suggesting resistance-like electrochemical behavior. As expected, electrode **B** exhibited substantially larger current density than electrode **A** because of its improved surface wettability and hierarchical structure. As the capacitance of a material is in proportion to the areas of its CV curves, the capacitance of **B** is larger than that of **A**. From the CV studies we have confirmed that electrode **B** has a stable voltage window between –1.0 and 0 V (*vs* Ag/AgCl) in $LiClO_4$ aqueous electrolyte. Thus **B** is a potential electrode material for application in supercapacitors. However, the specific capacitance of **B** decays significantly with the increasing sweep rates (Fig. 7d), which indicated that further tuning of the morphology is required in order future development of this material in energy storage devices.

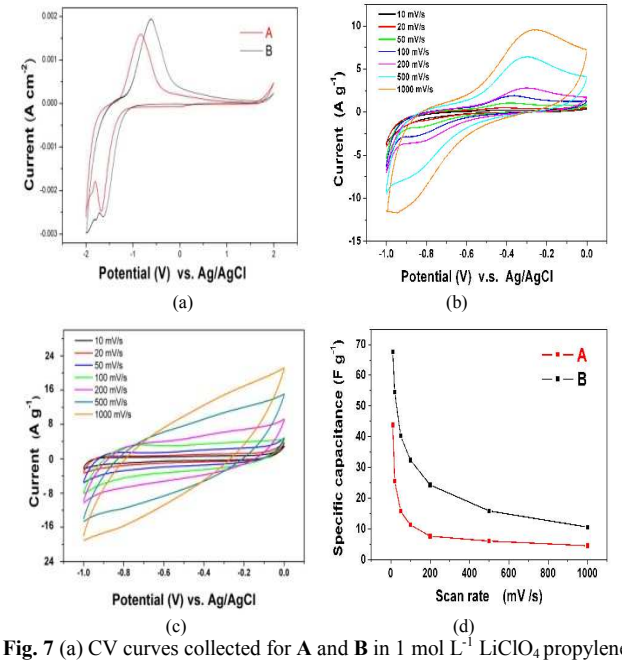

Fig. 7 (a) CV curves collected for **A** and **B** in 1 mol L^{-1} $LiClO_4$ propylene carbonate electrolyte; (b) CV curves of **A** at different scan rate in 1 mol L^{-1} $LiClO_4$ aqueous electrolyte; (c) CV curves of **B** at different scan rate in 1 mol L^{-1} $LiClO_4$ aqueous electrolyte; (d) Specific capacitance of **A** and **B** calculated from CV.

In summary, we have demonstrated a novel strategy to obtain nanoporous titania materials using the decomposition of POT cages, as exemplified using the new cage precursor $[Ti_2O(OAc)_2(HOAc)_2Cl_4]$ (**1**). The mesoporous TiO_2/carbon composite **A** and hierarchical nanoporous TiO_2/carbon composite **B** obtained using **1** show that the morphology and composition of these TiO_2/carbon composites can be drastically altered by the precise conditions of calcination (in the presence or absence of oxygen). Investigation of the electrochemical behaviors of **A** and **B** showed that the latter exhibits higher specific capacitance and will be an attractive supercapacitor material.

Acknowledgements: We thank National Natural Science Foundation of China (NSFC, No.51403060, 51003095 and 51103132), The EU (ERC advanced investigator award, DSW).

Notes and references

[a] International Science and Technology Cooperation Base of Energy Materials and Application, College of Chemical Engineering Zhejiang University of Technology, Hangzhou, 310014, P. R. China. Tel: 0086 571 88320253. E-mail: yaokanglv@zjut.edu.cn and czhang@zjut.edu.cn;
[b] Chemistry Department, Cambridge University, Lensfield Road, Cambridge CB2 1EW. Fax: 0044 1223 336362; Tel: 0044 1223 763122 E-mail: dsw1000@cam.ac.uk.
[c] Department of Materials chemistry, Huzhou University, Huzhou, 313000, P. R. China.

† Electronic Supplementary Information (ESI) available: *Synthesis, crystal data and analytic characterization of **1**. Synthesis and analytic characterization of **A** and **B**, EDS and XPS of **B**.* See DOI: 10.1039/b000000x/.

1 a) T. Brezesinski, J. Wang, J. Polleux, B. Dunn and S. H. Tolbert, *J. Am. Chem. Soc.* 2009, **131**, 1802–1809; b) Y. Lv, M. Yao, J. P. Holgado, T. Roth, A. Steiner, L. Gan, R. M. Lambert and D. S. Wright, *RSC Advances*, 2013, **3**, 13659-13662; c) K. Park, *Inorg. Chem.* 2005, **44**, 3190-3193.

2 a) X. Lu, G. Wang, T. Zhai, M. Yu, J. Gan, Y. Tong and Y. Li, *Nano Lett.*, 2012, **12**, 1690−1696; b) A. Ramadoss and S. J. Kim, *Carbon* 2013, **63**, 434−445.

3 a) X. Lu, M. Yu, G. Wang, T. Zhai, S. Xie, Y. Ling, Y. Tong and Y. Li, *Adv. Mater.*, 2013, **25**, 267–272; b) J. B. Wu, R. Q. Guo, X. H. Huang, Y. J. B. Wu, R. Q. Guo, X. H. Huang and Y. Lin, *Power Sources* 2013, **243**, 317-322; c) M. Cho, S. Park, K. Kimand, K. C. Roh, *Electron. Mater. Lett*, 2013, **9**, 809-812; d) M. Oh and S. Kim, *Electrochim. Acta*, 2012, **78**, 279– 285.

4 a) S. F. Pedersen, J. C. Dewan, R. R. Eckman and K. B. Sharpless, *J. Am. Chem. Soc.*, 1987, **109**, 1279-1282; b) Y. Lv, J. Cheng, A. Steiner, L. Gan and D. S. Wright, *Angew. Chem. Int. Ed.*, 2014, **53**, 1934-1938; c) Y. Lv, J. Cheng, P. D. Matthews, J. P. Holgado, J. Willkomm, M. Leskes, A. Steiner, D. Fenske, T. C. King, P. T. Wood, L. Gan, R. M. Lambert and D. S. Wright, *Dalton Trans.*, 2014, **43**, 8679-8689; d)Y. Lv, J. Willkomm, M. Leskes, A. Steiner, T. C. King, L. Gan, E. Reisner, P. T. Wood and D. S. Wright, *Chem-Eur J.*, 2012, **18**, 11867-11870; e) Y. Lv, J. Willkomm, A. Steiner, L. Gan, E. Reisner and D. S. Wright, *Chem. Sci.*, 2012, **3**, 2470-2473.

5 a) L. Rozes and C. Sanchez, *Chem. Soc. Rev.*, 2011, **40**, 1006–1030; b) F. Périneau, S. Pensec, C. Sassoye, F. Ribot, L. Lokeren, R. Willem, L. Bouteiller, C. Sanchez and L. Rozes, *J. Mater. Chem.*, 2011, **21**, 4470.

6 a) S. Brunauer, L. S. Deming, W. E. Deming and E. Teller, *J. Am. Chem. Soc.* 1940, **62**, 1723–1732; b) Y. Lv, L. Gan, M. Liu, W. Xiong, Z. Xu, D. Zhu and D. S. Wright, *J. Power Sources*, 2012, **209**, 152-157.

7 a) D. R. Rolison, *Science*, 2003, **299**, 1698–1701; b) J. Chmiola, G. Yushin, Y. Gogotsi, C. Portet, P. Simon and P. L. Taberna, *Science* 2006, **313**, 1760–1763.

8 a) Y. Jun, J. H. Park and M. G. Kang, *Chem. Commun.*, 2012, **48**, 6456–6471; b) T. Chen, P. J. Colver and S. A. F. Bon, *Adv. Mater.* 2007, **19**, 2286-2289; c) P. Yang, D. Zhao, D. I. Margolese, B. F. Chmelka and G. D. Stucky, *Nature*, 1998, **396**, 152–155; d) A. Verma, S. B. Samanta, N. C. Mehra, A. K. Bakhshib and S. A. Agnihotry, *Sol. Energ. Mat. Sol. C.*, 2005, **86**, 85–103.

9 a) T. Kang, D. Kima and K. Kim, J. *Electrochem. Soc.*, 1998, **145**, 1982–1986; b) A. Ghicov, S. P. Albu, J. M. Macak and P. Schmuki, *Small*, 2008, **4**, 1063–1066; c) S. Berger, A. Ghicov, Y. C. Nah and P. Schmuki, *Langmuir*, 2009, **25**, 4841–4844.

Graphical Abstract

From a polyoxotitanium cage to TiO_2/C composites, a novel strategy to nanoporous materials

J. Liu, Z. Cai, Y. Lv, Y. Zhang, S. Chang, M. Ouyang, C. Zhang and D. S. Wright

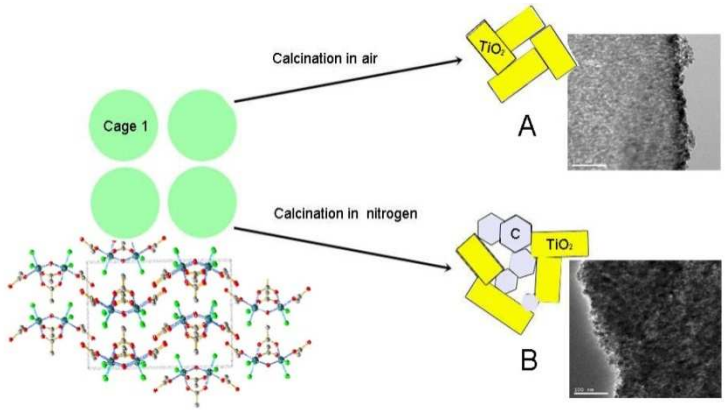

A novel strategy to obtain nanoporous titania materials through polyoxotitanium (POT) has been developed. Mesoporous TiO_2/carbon composite **A** and hierarchical nanoporous TiO_2/carbon composite **B** obtained using the new POT precursor $[Ti_2O(OAc)_2(HOAc)_2Cl_4]$, which show that the morphology and composition of these TiO_2/carbon composites can be drastically altered by the precise conditions of calcination. Investigation of the electrochemical behaviors of **A** and **B** showed that the latter exhibits higher specific capacitance and will be an attractive supercapacitor material.